Received: 11 September 2019 | Revised: 14 November 2019 | Accepted: 9 December 2019

DOI: 10.1002/mrm.28152

FULL PAPER

Magnetic Resonance in Medicine

Thermo-acoustic ultrasound for noninvasive temperature monitoring at lead tips during MRI

Neerav Dixit | **John M. Pauly** | **Greig C. Scott**

Department of Electrical Engineering, Stanford University, Stanford, CA, USA

Correspondence
Neerav Dixit, 350 Jane Stanford Way, Room 306, Stanford, CA 94305, USA.
Email: ndixit@stanford.edu

Funding information
National Institutes of Health, Grant/Award Number: 5R01EB012031, 2R01EB008108 and P01CA15999; William R. Hewlett Stanford Graduate Fellowship

Purpose: We explore the use of thermo-acoustic ultrasound (TAUS) to monitor temperature at the tips of conductive device leads during MRI.

Theory: In TAUS, rapid radiofrequency (RF) power deposition excites an acoustic signal via thermoelastic expansion. Coupling of the MRI RF transmit to device leads causes SAR amplification at lead tips, allowing MRI RF transmitters to excite significant lead tip TAUS signals. Because the amplitude of the TAUS signal depends on temperature, it becomes feasible to monitor the lead tip temperature during MRI by tracking the TAUS amplitude.

Methods: The TAUS temperature dependence was characterized in a phantom and in tissue. To perform TAUS acquisitions in an MRI scanner, amplitude modulated RF chirps were transmitted by the body coil, and the lead tip TAUS signal was detected by an ultrasonic transducer. The TAUS signal level was correlated with the RF current induced on the lead and the associated B_1 artifacts in MRI. TAUS signals acquired during RF-induced heating were used to estimate the lead tip temperature.

Results: The TAUS signal exhibited strong dependence on temperature, increasing over 30% with 10°C of heating both in the phantom and in tissue. A lead tip TAUS signal was observed for a 100 mA rms current induced on a lead. During RF-induced heating, the TAUS signal appeared to accurately approximate the peak lead tip temperature.

Conclusions: TAUS allows for noninvasive monitoring of lead tip temperature in an MRI environment. With further development, TAUS opens new avenues to improve RF device safety during MRI scans.

KEYWORDS

Active implantable medical devices, Implant heating, Interventional MRI, MRI engineering, RF safety, Thermo-acoustics

1 | INTRODUCTION

MRI of patients who have implanted medical devices with long conductive leads—including pacemakers, implantable cardioverter/defibrillators, and neurostimulators—is typically avoided due to the possibility of unsafe interactions between the strong radiofrequency (RF) fields used in MRI and the device leads. Coupling of these RF fields to the leads can induce significant currents on the leads, resulting in excessive RF power absorption and tissue heating at the

uninsulated lead tips.[1,2] Concerns regarding RF-induced heating have resulted in the designation of many implanted devices and leads as "MR unsafe," meaning scans should not be performed, and others as "MR conditional," indicating that scans should only be performed under certain conditions including limited RF power.[3] These restrictions prevent many implant recipients from receiving clinically useful MRI scans.

The interactions between the RF fields and a device lead depend on a number of factors, including the properties of the lead, the electrical properties of the tissue around the lead, and the geometric configuration of the lead and patient relative to the RF transmit coil.[4-8] In many cases, the degree of coupling of the RF transmit to a lead is not dangerous. Numerous patients who have implanted devices with leads susceptible to RF coupling have been scanned without issue using RF power levels above the manufacturer's recommended limits,[9-13] suggesting that many of those for whom scanning is restricted can actually be scanned safely at normal RF power levels. However, due to the complexity of the factors governing the interactions that cause RF-induced lead tip heating, making confident assertions about whether dangerous heating will occur for a particular case is difficult.

A reliable method to differentiate cases that are unsafe from those in which minimal heating will occur could allow many more patients to have access to MRI. A number of pre-scan techniques have been proposed to accomplish this without inducing dangerous temperature increases. Induced RF current on a lead creates an azimuthal magnetic field that distorts the nearby B_1 field. The magnitude[14-16] or phase[17,18] of these distortions enables estimation of the lead current. Reverse polarization of the body transmit/receive selectively visualizes these B_1 artifacts by suppressing the normal MRI tissue signal while retaining sensitivity to the B_1 distortions.[19] Another pre-scan method senses impedance perturbations of the transmit coil that are indicative of significant coupling.[20] Although initial results have been demonstrated using these methods, none have yet achieved widespread clinical adoption.

In addition to pre-scan screening, MR thermometry of lead temperature is feasible but difficult. Noninvasive MR thermometry has been performed during MR-guided focused ultrasound treatments.[21] However, MR thermometry techniques are less suitable for characterizing the peak temperature near a conductive lead. Thermometry methods based on the proton resonance frequency (PRF) shift phenomenon are sensitive to motion and fail near metal due to magnetic susceptibility artifacts,[22] and the accuracy of T_1-based MR thermometry suffers near lead tips due to B_1 artifacts caused by induced lead currents.[23] The highly localized RF power deposition at the lead tip also makes capturing the peak temperature with MR thermometry challenging, as obtaining data with sufficient spatial resolution requires long acquisition times, which further increases the RF exposure risk.

In this article, we propose the use of thermo-acoustic ultrasound (TAUS) to monitor the peak temperature at a lead tip during MRI. TAUS is based on the thermo-acoustic effect, in which RF power absorption induces acoustic waves via thermoelastic expansion.[24,25] The thermo-acoustic effect was first reported in an MRI setting when it was hypothesized to cause an auditory response in patients to RF pulses—RF power absorption in the brain created acoustic waves that reached the cochlea via bone conduction.[26] Using the MRI RF body coil transmit, we previously demonstrated TAUS detection of the strong local enhancement in RF power absorption at a lead tip associated with RF-induced heating.[27] However, in soft tissue, the TAUS signal amplitude also depends strongly on the tissue temperature. If the temperature dependence is known, the change in the TAUS signal amplitude from a lead tip can be used to estimate the tissue temperature rise at the lead tip in real time. Therefore, interleaving periodic TAUS acquisitions, performed using the MRI RF transmit system, with MR imaging can provide intrascan lead tip temperature monitoring. With noninvasive monitoring in this manner, unsafe MRI scans could be terminated before thermal damage occurs.

2 | THEORY

2.1 | The thermo-acoustic effect and TAUS

When a material absorbs RF energy, heating occurs and causes thermoelastic expansion. A pressure distribution arises, resulting in the propagation of acoustic waves from the site of RF absorption (Figure 1). This phenomenon is called the thermo-acoustic effect and is described by the inhomogeneous acoustic wave equation

$$\left(\nabla^2 - \frac{1}{v_s^2}\frac{\partial^2}{\partial t^2}\right) p(\vec{r},t) = -\frac{\beta\rho}{C} G(\vec{r}) \frac{\partial P(t)}{\partial t}, \qquad (1)$$

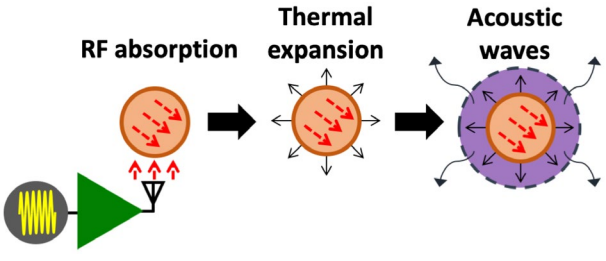

FIGURE 1 In the thermo-acoustic effect, pulsed RF power deposition causes rapid thermal expansion and the emission of acoustic waves

in which the local specific absorption rate $\mathrm{SAR}(\vec{r},t) = G(\vec{r})P(t)$ is separable under narrow band RF conditions. G is the SAR spatial profile from the RF transmit, and P is the RF transmit power over time, which is proportional to the square of the RF transmit amplitude. Here, p is the generated thermo-acoustic pressure in a medium for which v_s is the speed of sound, β is the thermal expansion coefficient, ρ is the density, and C is the specific heat.

In TAUS, the acoustic signals excited from an RF transmit via the thermo-acoustic effect are detected to characterize the RF power absorption. To perform TAUS acquisitions, the MRI RF transmit must excite acoustic signals that are at appropriate frequencies for detection by ultrasonic receivers and allow for spatial localization of acoustic sources. The linear relationship between the thermo-acoustic pressure and the RF transmit power in Equation 1 means that the excited acoustic signals have a square law relationship with the RF transmit signal. Therefore, the frequency content of the RF transmit envelope, rather than the RF carrier frequency, determines the frequency content of the acoustic signal.

Using this principle, TAUS acquisitions have been performed with multiple RF transmit modulation schemes, and we compared some of these techniques previously.[27] Frequency-modulated continuous-wave (FMCW) methods, in which frequency encodes depth, were superior to time-domain pulsed acquisitions. For FMCW TAUS excitations, an RF carrier is amplitude-modulated by a chirp signal that sweeps through the desired acoustic excitation frequencies.[28] The modulation can be traditional amplitude modulation (FMCW amplitude modulation) or on/off keying (OOK) from a square wave that follows the chirp frequency (FMCW square wave modulation). The instantaneous frequency of a chirp signal of duration T is $f_c(t) = f_0 + Bt/T$, where f_0 is the initial frequency of the chirp and B is its frequency span. During RF transmit, TAUS signals of frequency $f_c(t)$ are excited and propagate as acoustic waves. As illustrated in Figure 2, for a signal excited at distance d from an acoustic receiver, the propagation delay causes the instantaneous frequency of the signal observed by the receiver to be $f_{rx}(t) = f_c(t - d/v_s)$. When this received signal is mixed with the original chirp signal, a signal is generated whose frequency content is the difference between the two signals' frequencies, $f_c(t) - f_{rx}(t)$. This yields a beat frequency f_b proportional to d, such that $f_b = Bd/(Tv_s)$. Windowing followed by a Fourier transform reveals the TAUS signal versus distance from the receiver.

2.2 | TAUS signal from a lead tip in an MRI setting

If the MRI RF transmit couples to a device lead, current is induced on the lead, and the SAR near the lead tip is amplified significantly above that of the surrounding tissue. Equation 1 shows that the initial thermo-acoustic pressure distribution matches $G(\vec{r})$, the spatial profile of the local SAR. As was demonstrated previously,[27] the MRI body coil can excite strong TAUS signals at lead tips.

Simple analytical relationships between the induced current and the resulting SAR are possible for the ideal case of an infinitely thin insulated wire driving a current with root mean square (rms) value I_{rms} into a spherical electrode immersed in homogeneous tissue (Figure 3). At distance r from the center of a spherical electrode with radius R_0, the current density, time-averaged SAR, and worst-case steady-state temperature rise (derivation shown in Appendix A) around the electrode ($r \geq R_0$) are given by:

$$\vec{J}(r) = \frac{I}{4\pi r^2}\hat{r}, \tag{2}$$

$$\mathrm{SAR}(r) = \frac{I_{\mathrm{rms}}^2}{16\pi^2 r^4 \sigma \rho}, \tag{3}$$

$$\Delta T(r) = \frac{I_{\mathrm{rms}}^2}{16\pi^2 \sigma k R_0}\left[\frac{1}{r} - \frac{R_0}{2r^2}\right], \tag{4}$$

where ρ, σ, and k represent, respectively, the density, electrical conductivity, and thermal conductivity of the tissue. The initial temperature rise is simply $\Delta T(r) = C^{-1}\mathrm{SAR}(r)dt$, and the initial pressure rise caused by the thermo-acoustic effect is $p_0(r) = \beta v_s^2 C^{-1}\rho \mathrm{SAR}(r)dt$. The wire current will also perturb the MR nutation frequency by $\Delta f_n \approx 6.02 I_{\mathrm{rms}}/r$ Hz.

For context, consider the case of $I_{\mathrm{rms}} = 20$ mA driving a spherical electrode ($R_0 = 1$ mm) that is immersed in tissue,

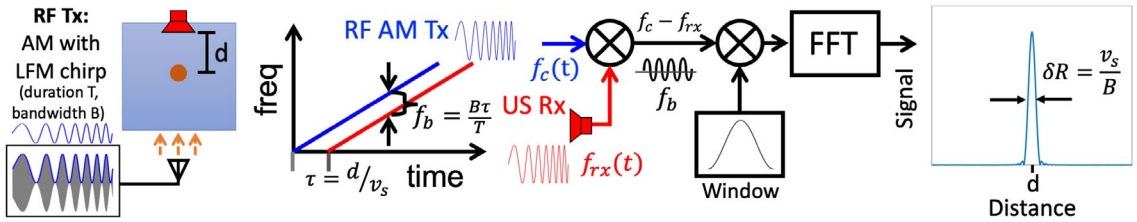

FIGURE 2 Illustration of a TAUS acquisition using FMCW amplitude modulation. This example shows RF absorption at a point source located distance d from an acoustic receiver. Mixing of the received acoustic signal with the original chirp signal used for amplitude modulation yields a beat frequency f_b which is proportional to d

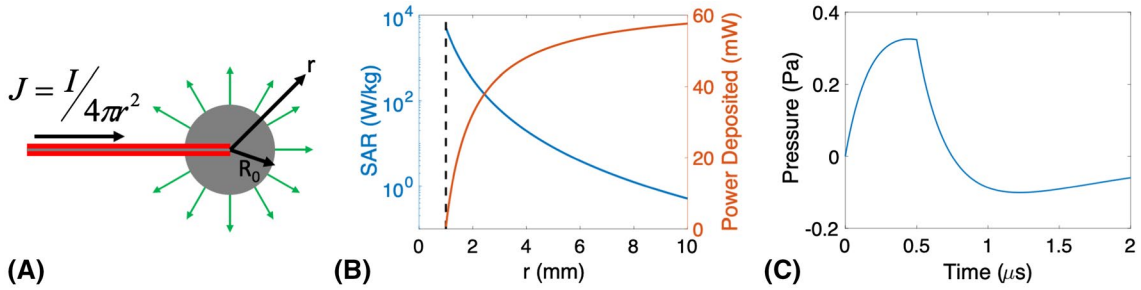

FIGURE 3 A, Illustration of the model in which current is driven by a thin insulated wire into a spherical electrode. B, SAR versus radial position and total power deposited within a sphere of radius r for the case of $I_{rms} = 20$ mA and $R_0 = 1$ mm. The dotted line shows the position of the electrode surface. C, Pressure waveform excited at the electrode surface ($r = R_0$) from a 500 ns pulse of current for the case described in part B

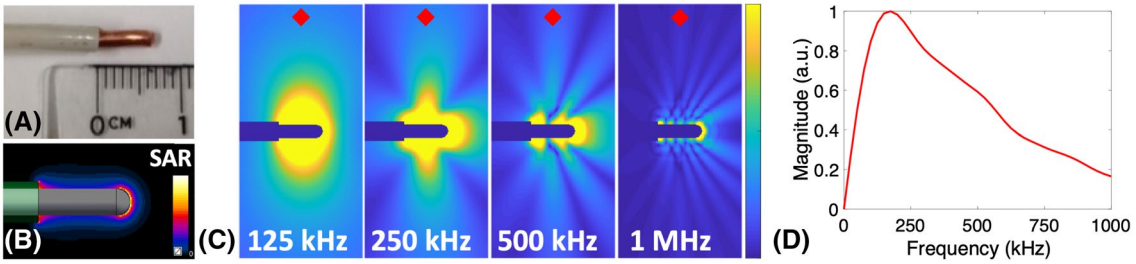

FIGURE 4 A, Model lead tip. B, Simulated SAR distribution at the lead tip from a 64 MHz transmit. C, TAUS acoustic fields generated from continuous wave amplitude modulation of the 64 MHz transmit at various modulation frequencies and equal drive power. D, Relative magnitude of the generated acoustic field as a function of the modulation frequency at the point labeled with the red diamond in part C

with $\rho = 1000\,\text{kg/m}^3$, $\sigma = 0.5$ S/m, and $k = 0.5$ W/m/K. Equation 3 implies that the total power dissipated into the tissue is about 64 mW, and Equation 4 shows that the worst-case steady-state temperature rise at the electrode surface is 5°C. Due to the extreme local amplification in SAR—the SAR value is approximately 5 kW/kg at the surface of the electrode while being only 8 W/kg 4 mm away—50% of the power is delivered within 1 mm of the electrode surface (Figure 3B).

The excited thermo-acoustic pressure increases dramatically near the electrode because of the local SAR amplification. A 500 ns pulse of current with $I_{rms} = 20$ mA will generate a peak thermo-acoustic pressure of about 0.33 Pa at the electrode surface in soft tissue (Figure 3C), with a peak temperature rise of 0.63 μK. Averaging will improve the TAUS SNR; for example, 2500 averages improves SNR 50× while increasing the worst-case heating at the electrode surface to about 1.6 mK. The thermo-acoustic pressure scales linearly with power; a 5× increase in the induced current to $I_{rms} = 100$ mA will increase the power by 25×, so that a 500 ns pulse now generates a peak thermo-acoustic pressure of about 8.25 Pa at the electrode surface with a 16 μK peak temperature increase.

The SAR spatial profile of more general lead geometries affects the properties of the acoustic signal that propagates from the lead tip.[27] Interference patterns form in the propagating acoustic waves according to both the source geometry of the TAUS signal imposed by the SAR spatial profile and the wavelengths of the excited acoustic frequencies. Multiphysics RF and acoustic simulations allow for characterization of these variations as a function of the excited acoustic frequencies.[27] Figure 4 shows both the simulated SAR spatial profile and the simulated acoustic fields at various acoustic frequencies for a model lead tip excited with a 64 MHz RF signal. With knowledge of the TAUS signal propagation as a function of excited acoustic frequency, an appropriate modulation bandwidth for the RF transmit can be selected to maximize the acquired lead tip TAUS signal.

2.3 | TAUS for lead tip temperature monitoring

In soft tissue, the thermal expansion coefficient β varies significantly with temperature, as does the speed of sound v_s. Consequently, according to Equation 1, the amplitude of the TAUS signal will vary with local tissue temperature. The strong temperature dependence of the TAUS signal in tissue has been demonstrated in several studies.[29-33]

The TAUS temperature dependence creates a new avenue for lead tip temperature monitoring in MRI. For a given tissue type, the functional change in signal amplitude with temperature $F(T)$ should not depend on the transmit and receive setup

for TAUS acquisitions. Therefore, the same relative change in TAUS signal with temperature would be expected when using a test setup to characterize F for a particular tissue type and when acquiring a TAUS signal in an MRI setting from a lead tip immersed in that tissue. The lead tip TAUS signal can then be expressed as

$$S(T) = \alpha F(T), \tag{5}$$

where α is a scalar factor that expresses the scaling in signal amplitude between S and F. Once F has been characterized, α can be determined with a calibration scan in which the signal S is acquired at a known initial lead tip temperature. Then, future acquisitions of S can provide estimates of the temperature at the lead tip by inverting the function, so

$$T = F^{-1}\left(\frac{S}{\alpha}\right). \tag{6}$$

Because the highest temperatures caused by RF-induced lead tip heating occur at the same SAR hotspots that contribute most to TAUS signal generation, the temperature estimated by TAUS monitoring should represent the peak temperature at the lead tip.

To perform accurate lead tip temperature monitoring with this technique, the temperature dependence of the lead tip TAUS signal must closely match the function F used in Equation 6. The lead tips of implanted medical devices must be precisely positioned for the device leads to perform their intended functions, meaning that the type of tissue in contact with a lead tip—which should be used to measure F—is known with a high degree of confidence. For a lead tip partially immersed in both fat and the desired aqueous tissue, the much higher electrical conductivity of the aqueous tissue likely means that it will experience a significantly higher local SAR. Consequently, the TAUS signal would originate mostly from this tissue, and its TAUS temperature dependence would be used for lead tip temperature estimation. Ensuring accurate temperature estimation with TAUS may ultimately require the creation of a database that catalogs the properties of different tissues, as has been done for tissue dielectric properties.

3 | METHODS

3.1 | Characterization of TAUS temperature dependence

The TAUS temperature dependence was characterized in a saline gel phantom (distilled water, 8 g/L polyacrylic acid, 0.7 g/L sodium chloride, doped with nickel chloride) and in chicken breast tissue using the setup illustrated in Figure 5. A TAUS signal source and fiber optic temperature probes (FOT-L-NS-967C, FISO Technologies, Inc., Quebec, Canada) connected to a signal conditioner (DMI, FISO Technologies Inc.) were immersed in each medium to be characterized. The medium was then placed in a water bath, which was heated by a hot plate while TAUS acquisitions were performed. The saline gel phantom was contained in a glass container placed in the water bath, whereas the piece of chicken breast was covered in a plastic wrap.

To serve as a TAUS signal source, one end of a coaxial cable was stripped to expose the center conductor, on which a solder ball was electrically connected. FMCW TAUS acquisitions were performed using a square-wave-modulated RF transmit into the cable to excite a TAUS signal at the solder ball. To generate the transmit waveform, an Analog Discovery 2 module (Digilent, Inc., Pullman, Washington)—a programmable oscilloscope that includes two arbitrary waveform generators (AWG)—transmitted a linear frequency modulated chirp signal of 2.5 ms duration spanning 250-750 kHz. The chirp signal triggered a LT1016 comparator to create an approximate 50% duty cycle chirped square wave. The square wave acted

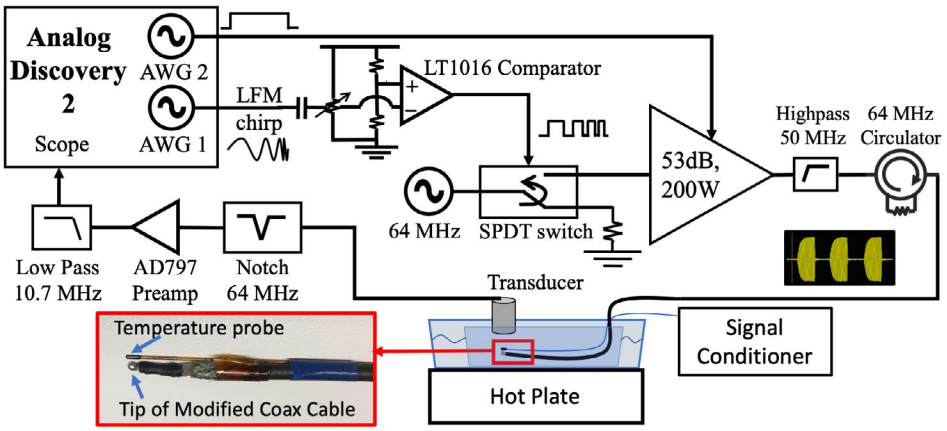

FIGURE 5 Diagram of the test setup used to characterize the TAUS signal level versus temperature in different media

as a gating signal for a ZASWA-2-50DR+ SPDT switch controlling a 64 MHz RF input signal. The resulting square-wave-modulated RF signal was amplified by a 200 W power amplifier (AR Kalmus model LA200HP-CE, 0.5–100 MHz) before driving the modified coaxial cable. To avoid temperature differences between the fiber optic probes near the coax tip TAUS source and the coax tip itself, a very low transmit duty cycle minimized local heating—one 2.5 ms RF transmit was performed every 10 s at peak powers well below the 200 W rating of the power amplifier. Temperature changes in the medium and at the coax signal source occurred primarily from uniform heating of the surrounding water bath by the hot plate.

An Olympus V318-SU 0.5 MHz immersion ultrasonic transducer received the TAUS signal, followed by a notch filter at 64 MHz to suppress RF carrier intermodulation effects. The signal was amplified by an AD797-based preamplifier, low pass filtered (Mini-Circuits BLP-10.7+), and digitized in an oscilloscope channel of the Analog Discovery 2.

FMCW postprocessing of the digitized signal recovered the signal level versus distance. The TAUS signal peak, corresponding to the lead tip, was tracked over time during uniform heating of the medium. The TAUS signal versus temperature relationship was then determined for both media. In each case, an affine model was fitted to the data to approximate this relationship.

3.2 | TAUS signal and B_1 artifacts from lead current induced by body coil transmit

The setup shown in Figure 6 used the body coil of a GE Signa 1.5T MRI scanner to excite a TAUS signal from the tip of an in-bore model lead, while the induced current on the lead was measured. Gradient echo MR imaging, during which the induced lead current was also measured, was performed as well to observe the B_1 artifacts caused by this current. Additionally, the lead current was independently estimated using double-angle gradient echo imaging. These tests related the induced lead current that generates a detectable lead tip TAUS signal to the lead current associated with B_1 artifacts in MRI.

The FMCW square wave modulation electronics were interfaced with the MRI body coil amplifier input to generate an FMCW B_1 envelope in the body coil when running a dummy MRI sequence. When the scanner triggered the Analog Discovery 2 controller, a 2.5 ms duration FMCW RF signal was broadcast into the body coil amplifier. The RF carrier frequency was set to the Larmor frequency, and the modulation frequency increased linearly in time from 250 to 750 kHz. The body coil B_1 was sensed by a pickup loop placed in the scanner bore and displayed on an oscilloscope.

A 170-cm long insulated 12 AWG copper wire with 7 mm of insulation stripped at one end acted as a model device lead.

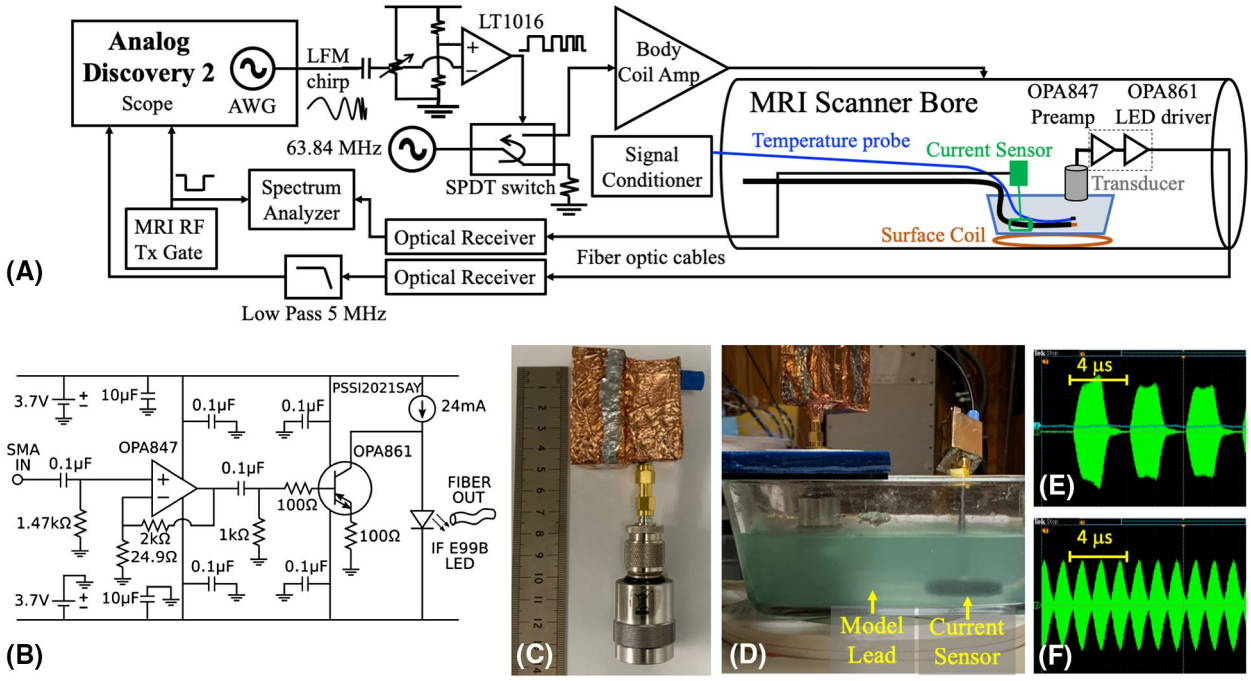

FIGURE 6 A, Diagram of the setup used during TAUS acquisitions in the MRI scanner. The surface coil and current sensor were only present in the tests relating the TAUS signal to the induced lead current and MRI B_1 artifacts, whereas the temperature probe was only present in the test in which the TAUS signal was used to estimate the lead tip temperature. B, Schematic of the preamplifier and LED driver circuits. C, Shielded box containing the preamplifier and LED driver attached to the 0.5 MHz ultrasonic transducer. D, Model lead, current sensor, and ultrasonic transducer in the saline gel phantom. (E, F) Square-wave-modulated RF transmit received by a pickup loop in the body coil at modulation frequencies of (E) 250 kHz and (F) 750 kHz

The lead tip and approximately 15 cm of the model lead were immersed in the saline gel phantom, which was placed on top of a 5-inch surface coil. The lead tip was positioned near the isocenter of the MRI bore.

The same 0.5 MHz ultrasonic transducer used to characterize the TAUS temperature dependence was positioned with its surface immersed in the phantom above the model lead tip to receive excited TAUS signals. An RF-shielded box, which was attached to the transducer, contained an OPA847-based preamplifier and an OPA861-based RC-LED driver, along with two LiPo 3.7 V nonmagnetic batteries. A plastic fiber optic cable connected the output of the LED driver to one of two photoreceiver channels in the console room, each of which used circuitry described in Zanchi et al.[34] The output of the photoreceiver channel was low-pass filtered (Mini-Circuits BLP-5+) before being digitized by the Analog Discovery 2.

An optically coupled current sensor similar to Etezadi-Amoli et al,[16] but now LiPo battery-powered, monitored the lead current induced by the body coil transmit. The toroidal sensor was placed over the lead and was centered about 8 cm behind the uninsulated lead tip. The fiber optic output of the current sensor was interfaced over plastic fiber to a second photoreceiver channel in the console room. A Tektronix RSA306 spectrum analyzer, centered at the Larmor frequency, displayed the time-domain power level of the photoreceiver output during each RF transmit. In a prior calibration procedure, power readings were recorded with the sensor placed over a wire of known current and signal source, allowing the conversion of spectrum analyzer readings to rms current values on the model lead.

Because TAUS acquisitions were performed during dummy MRI sequences, the scanner's gradient coils were active, despite not being relevant to the TAUS signal. These gradients coils appeared to interfere with the TAUS receive setup in the scanner bore, as harmonics of the gradient amplifier switching frequencies were observed at significant levels in the receive signal. To reduce this interference, separate TAUS acquisitions were performed with the FMCW RF signal on and off, allowing subtraction of the gradient interference in postprocessing. Eighty averages of TAUS acquisitions with a square-wave-modulated RF transmit were performed, and another 80 were performed with no RF transmit.

Following the TAUS acquisitions, the lead flip angle distortion was analyzed using axial double-angle gradient echo imaging.[35] For imaging, the ultrasonic transducer was removed from the phantom to avoid susceptibility artifacts caused by its stainless steel case. The positioning of the model lead and current sensor were unchanged between the TAUS acquisitions and the MR imaging, so that body coil RF coupling to the lead was the same in both cases.

Three slices that included cross sections of the lead were acquired with B_1 power levels set to induce 15° and 30° flip angles in the phantom far from the wire. For both power levels, gradient echo imaging was performed with parameters: 5 mm slice thickness, 0.625 mm in-plane resolution, 15 mm slice separation, TE 10 ms, and TR 1 s. The model lead was positioned approximately parallel to the diameter of the 5-inch surface receive coil to minimize receive coupling. The transmit field distortion of B_1 around an axially oriented wire with current I(t) results in a local flip angle:

$$\theta_w = \gamma \int \left| B_1^+(t) - j\frac{\mu_0 I(t)}{4\pi r} e^{j(\alpha-\phi)} \right| dt, \tag{7}$$

where γ is the gyromagnetic ratio, α is the phase of the wire current relative to B_1, ϕ is the angular position in the plane, and r is the radial distance from the wire center.[14] The current sensor, positioned as it was during the TAUS acquisition, independently quantified the induced sinc pulse envelope ($|I(t)|$) on the lead during imaging. After accounting for the sidelobe phase reversal, the expected flip angle distortion around the wire was calculated from Equation 7.

The distortion level expected according to the current sensor measurements was compared with the distortion level observed on the flip angle maps obtained using the double-angle method. To quantify the observed distortion level for each slice from its flip angle map, the center of the wire signal void determined the local origin for analysis ($r = 0$ in Equation 7). A script was written in MATLAB to find the magnitude and phase of the distortion modeled in Equation 7 that minimized the error between the modeled and measured flip angles in a region around the wire. Voxels with low MR signal intensity, including those at the wire location and those at the induced signal null near the wire, were excluded from the analysis due to the poor performance of the double-angle method for low SNR and low flip angle data.

3.3 | TAUS lead tip temperature estimation in MRI scanner

Using the same MRI-TAUS interface, TAUS signals were acquired from the lead tip using high/low duty cycles to demonstrate TAUS tracking of heating and cooling at the lead tip. The lead tip was positioned in the phantom as before, but without a current sensor. A temperature probe was secured near the lead tip to record the temperature over time. The lead path in the scanner bore was configured to induce much more coupling of the body coil RF transmit to the lead than in the prior tests. With this increased coupling creating a much stronger TAUS excitation, signal averaging and subtraction of gradient interference were not required to observe a clear lead tip TAUS signal.

The increased coupling also allowed the body coil FMCW transmission to serve as a proxy for an MR pulse sequence that could induce significant heating at the lead tip. TAUS acquisitions were initially performed at low duty cycle (one 2.5 ms FMCW excitation every 1 s) to obtain signals without

appreciable heating. The duty cycle was then increased by a factor of 20 (one 2.5 ms FMCW excitation every 50 ms) to stimulate lead tip heating while acquiring TAUS signals. Following a 5-minute heating period, the duty cycle was decreased to its initial level to acquire TAUS signals during cooling at the lead tip.

The TAUS acquisitions performed at low duty cycle prior to heating and the initial temperature probe reading were used to calibrate the previously determined model relating the temperature in the phantom to the TAUS signal level. Using this calibrated model, estimates of the lead tip temperature were obtained from the TAUS signal levels during the heating and cooling periods.

3.4 | Simulation of temperature profile around model lead tip

A simulation in COMSOL Multiphysics (COMSOL, Inc., Burlington, Massachusetts) estimated the temperature distribution around the model lead tip immediately following the 5-minute period of lead tip heating during the TAUS acquistions in the MRI scanner. A 2D axisymmetric geometry (2D cylindrical coordinates with azimuthal symmetry) was utilized for the simulation. First, the SAR spatial profile around the lead tip was characterized with a frequency-domain electromagnetic simulation at 64 MHz using a source placed along the lead insulation far from the uninsulated lead tip. The copper wire was modeled as a perfect electric conductor, the insulation was modeled with a relative permittivity of 3 and no electrical conductivity, and the surrounding medium was modeled with a relative permittivity of 78 and an electrical conductivity of 0.5 S/m.

A heat transfer simulation was then performed using the simulated SAR spatial profile as the input power distribution. The medium was simulated with a thermal conductivity of 0.5 W/m/K, a density of 1000 kg/m3, and a specific heat of 4000 J/kg/K. No heat flow was permitted into the lead conductor and insulation, and no perfusion was modeled. A constant power over time was simulated over the same 5-minute heating duration used in the TAUS lead tip temperature estimation experiment, and the power level was chosen to induce the same peak temperature increase as was estimated by the TAUS acquisition.

4 | RESULTS

4.1 | Characterization of TAUS temperature dependence

Figure 7 shows the TAUS signal amplitude and temperature over time as the characterized media were heated, as well as the variation in TAUS amplitude versus temperature. The TAUS amplitude exhibited a strong temperature dependence in both the saline gel phantom and the chicken breast tissue, increasing by over 30% with a 10°C temperature rise in both cases. The modeled affine fit agreed closely with the data ($r^2 = 0.993$ in the phantom and $r^2 = 0.983$ in the chicken breast). The apparent affine behavior of the TAUS signal amplitude in tissue matches observations reported elsewhere.[29,31,32]

4.2 | TAUS signal and B_1 artifacts from lead current induced by body coil transmit

Figure 6E,F show the body coil B_1 waveform measured by the pickup loop during the square-wave-modulated RF transmit. Due to the high Q of the body coil, the envelope of the

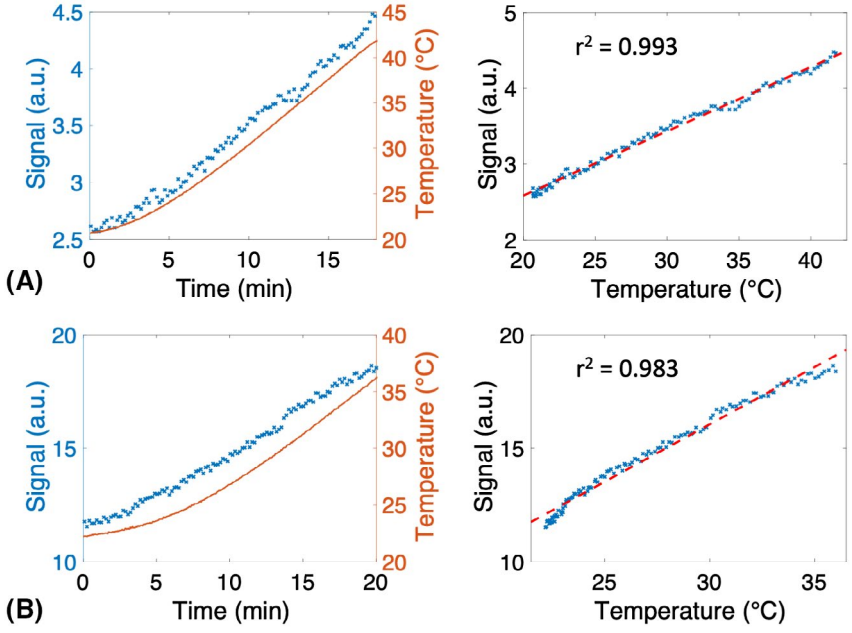

FIGURE 7 Plots of TAUS signal and temperature versus time as well as TAUS signal versus temperature for the coax tip TAUS signal source in the (A) saline gel phantom and (B) chicken breast tissue. The red dotted line on the signal versus temperature plot shows the affine fit to the data, and the associated r^2 values are displayed

RF transmit changed from a square wave as the amplitude modulation frequency increased.

The current sensor measurement of the rms lead current is plotted in Figure 8A for the RF transmit signals used in the TAUS acquisition and in gradient echo imaging with 15° and 30° flip angles. Because the induced lead current is linear with B_1, these measurements indicate that the transmit power throughout the 2.5 ms FMCW square-wave-modulated RF transmit was near the peak transmit power of the 30° RF pulse from MR imaging. At this RF transmit power, about 100 mA_{rms} was induced on the model lead.

Figure 8B shows the TAUS signal obtained by taking the difference between the averaged signal of 80 acquisitions using FMCW square wave modulation and the averaged signal of 80 acquisitions without any RF transmit. Direct feedthrough of the body coil transmit to the in-bore receive electronics manifests as a strong peak at zero distance. The lead tip signal can be observed at the distance between the transducer and the model lead tip, and reflections of the lead tip signal from the walls and surface of the phantom appear as echoes.

One of the acquired gradient echo images from an acquisition using a 15° flip angle is displayed in Figure 8C, with a clear flip angle artifact around the model lead. The flip angle map around the lead tip, obtained using the double-angle method, is shown in Figure 8D. For the 15° gradient echo acquisition, the current sensor indicated a peak I_{rms} of 50.5 mA, and calculations using the sensor data indicated an expected maximum flip angle distortion of 44° at 2 mm distance from the lead center, with a 1/r falloff in B_1 distortion as described in Equation 7. Fitting of the flip angle distortion model in Equation 7 to the double-angle flip angle maps resulted in estimated distortion levels that would create 46.5°, 48.5°, and 53° flip angle distortions 2 mm from the lead center. These estimates would correspond to peak I_{rms} values of 53.4 mA, 55.7 mA, and 60.9 mA during the RF excitation, an average deviation of 12% from the current sensor value.

4.3 | TAUS lead tip temperature estimation in MRI scanner

Figure 9A shows the lead tip TAUS signal and the nearby temperature probe reading over time for the body coil transmit test that was devised to induce significant lead tip heating. Figure 9B shows the peak lead tip temperature over time estimated from the TAUS signal level using the calibrated affine model for the TAUS signal versus temperature in the phantom. During the heating process, the TAUS-estimated peak lead tip temperature exceeded the temperature recorded

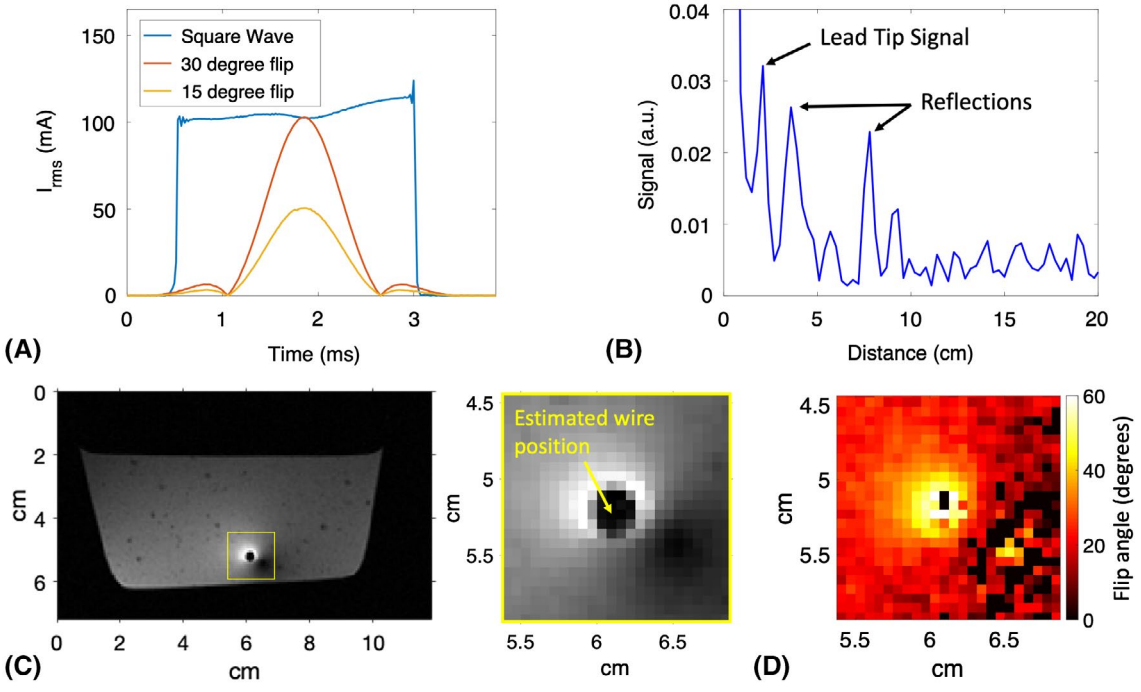

FIGURE 8 A, Root mean square current on the model lead measured by the current sensor during the FMCW square-wave-modulated RF transmit, the 30° RF pulse, and the 15° RF pulse. B, Measured signal versus distance from the transducer for the TAUS acquisition. A strong signal is present at zero distance due to direct feedthrough of the RF transmit to the receive electronics. Reflections of the acoustic signal occurred from the walls and surface of the phantom. C, Gradient echo MR image, obtained using a 15° flip angle, showing a cross section of the model lead and the flip angle artifact nearby. A magnified view of the region enclosed in the box shows the estimated center point of the wire. D, Flip angle map obtained for the magnified region around the wire in part C. A clear amplification in the flip angle is present on one side of the wire. Flip angle estimates in the regions with a low magnitude MR signal are unreliable and were not used to quantify the induced B_1 distortion levels

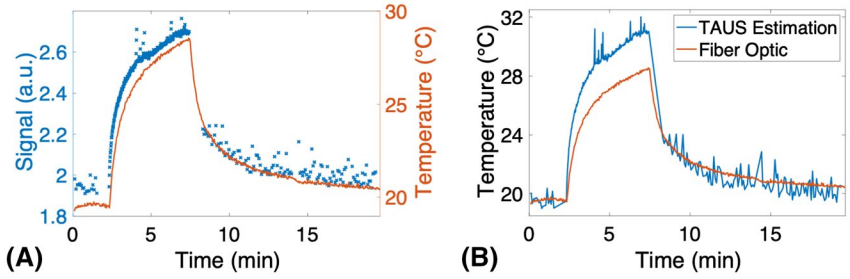

FIGURE 9 A, TAUS signal from the model lead tip and temperature measured by the nearby fiber optic temperature probe during the test involving lead tip heating and cooling. B, Lead tip temperature estimated by the TAUS signal level over time using a calibrated version of the affine model in Figure 7A, and the temperature probe measurement over time

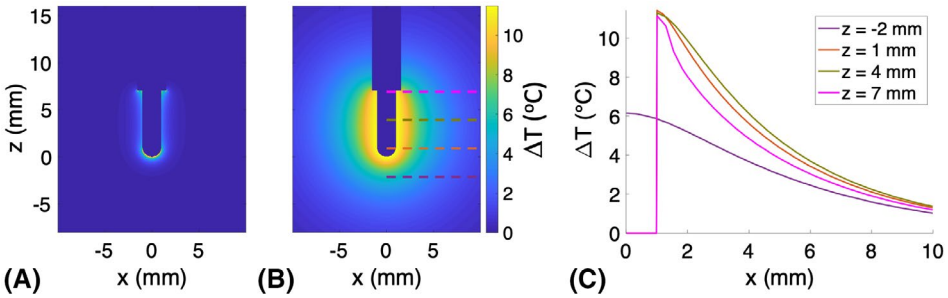

FIGURE 10 A, Simulated SAR spatial profile at the lead tip for a cross section through the center of the lead. B, Simulated temperature profile in the cross section. C, One-dimensional plots of the temperature along horizontal slices through the temperature distribution in part B. Only half of each slice is plotted due to symmetry

at the nearby fiber optic temperature probe, with a difference of 2.5℃ at the end of the heating period.

4.4 | Simulation of temperature profile around model lead tip

Results from the electromagnetics and heat flow simulations performed in COMSOL Multiphysics are displayed in Figure 10. The concentrated SAR profile resulted in significant temperature gradients around the lead tip immediately following the heating period; the temperature at a point on the lead tip surface was 4.2℃ above the temperature at a point 2 mm away.

5 | DISCUSSION

For the TAUS acquisitions performed in the MRI scanner, the TAUS receive electronics were subject to interference from both the body coil RF transmit and the gradient coils. Although the TAUS signals were acquired at much lower frequencies than the RF transmit, nonlinear distortion in the receive chain of any coupled RF transmit signal effectively demodulates the square wave envelope, creating a feedthrough signal at zero depth. After performing FMCW postprocessing for TAUS acquisitions, the sidelobes of an excessive feedthrough signal could exceed the actual noise level from the ultrasonic transducer, limiting the observed SNR and preventing improvements through signal averaging. Coupling of signals from the gradient switching frequency harmonics within the bandwidth used for the square wave modulation could also result in background interference levels above the noise floor. An effort was made to minimize interference through electromagnetic shielding of the TAUS preamplifier, as well as by transmitting the amplified receive signal fiber optically out of the scanner bore. Further reductions in the interference levels could potentially be achieved with better shielding of the transducer and the attached receive electronics as well as through notch filtering of the RF signal at the preamplifier input. The gradients can also be programmed to remain inactive during TAUS acquisitions.

Using the quantified sensor currents, measured lead tip TAUS signal, and gradient echo MR images, the level of RF coupling that induces B_1 artifacts can be related to the coupling that generates a detectable lead tip TAUS signal. The results in Figure 8 indicate that even when the MRI transmit induces lead currents that create relatively minor local B_1 distortions, FMCW TAUS acquisitions of comparable RF power levels generate lead tip TAUS signals that can be detected and localized.

The TAUS-estimated lead tip temperature in Figure 9B exceeded the temperature at the fiber optic probe positioned near the lead tip during heating. Here, the extremely localized

nature of lead tip heating—demonstrated by the simulation results in Figure 10—suggests that even a millimeter-scale separation between the probe and the lead tip may cause the temperature probe to significantly underestimate the actual peak lead tip temperature during heating. Temperature probes can never be positioned directly at a lead tip and therefore cannot be used to reliably assess the maximum temperature increase in these extremely localized heating scenarios. In contrast, the TAUS signal originates directly from the regions in which maximum heating occurs, so estimation of the lead tip temperature from the TAUS signal can actually capture the peak temperature.

To achieve TAUS monitoring of the peak lead tip temperature during an MRI scan, integration of TAUS acquisitions with MRI pulse sequences should be possible with minimal impact on the MRI scan. TAUS acquisitions can be performed in milliseconds; hence, they can be inserted during otherwise unused times in MRI pulse sequences. They can be designed to avoid disrupting the precession of the magnetization; using an off-resonant RF transmit should prevent any RF spoiling, and gradient fields are not required in TAUS. Although adding TAUS to MRI scans would increase the total RF transmit energy, TAUS signals can be generated at lead tips with minimal heating, as demonstrated by the initial low RF duty cycle acquisitions shown in Figure 9 that were performed prior to heating.

A number of potential obstacles to in vivo TAUS acquisitions from lead tips must be addressed before this technique can be used reliably in MRI. One challenge is the effective placement of an ultrasonic transducer on a patient who must be positioned in an MRI scanner. The transducer's acoustic coupling to the patient and its positioning relative to the lead tip will have a strong impact on the observed TAUS signal level. The TAUS temperature tracking property, however, is based on ratio-metric signal levels. The transducer also must be designed from MRI-compatible materials and should not induce strong image artifacts. The acquisition of both ultrasound and MRI signals without a strong sensitivity to transducer alignment or position has been demonstrated.[36]

Lead tips may also be located in the body such that obtaining a clear acoustic window for unimpeded acoustic wave propagation between the tip and transducer is impractical. Although obstacles in the signal path will diminish the observed TAUS signal level, clinical usage of transcranial focused ultrasound (tcFUS) has demonstrated that acoustic signals can maintain appreciable power levels after propagating through reflecting and attenuating structures such as the skull.[37] Like tcFUS, TAUS only requires one-way acoustic propagation and can be performed using relatively low acoustic frequencies (<1 MHz) to minimize signal loss due to attenuation. Acoustic insertion loss through bone increases with frequency; the one-way insertion loss through a human skull is typically about 10 dB at 500 kHz, compared to about 20 dB at 1.5 MHz.[38] In this work, we used acoustic signals from 250-750 kHz for lead tip TAUS acquisitions. The use of multiple transducers or a transducer array for TAUS could also allow for improved SNR through receive focusing at a known lead tip position. The feasibility of transcranial TAUS signal detection has been demonstrated recently using ex vivo human skulls.[39,40]

Additionally, because the TAUS signal is proportional to SAR, detecting a clear TAUS signal in cases without strong SAR amplification at the lead tip will require a sensitive detection setup. The TAUS system sensitivity will depend largely on the properties of the ultrasonic receivers; in this work, a relatively inexpensive transducer designed for nondestructive testing was employed. Characterizing the expected TAUS frequency response from a specific lead tip SAR pattern could also boost SNR through specific matched filtering of the received signal.

6 | CONCLUSIONS

The characterization of the TAUS signal behavior and the demonstration of lead tip temperature estimation using TAUS in an MRI scanner suggests that TAUS is a promising tool for the detection of dangerous RF-induced lead tip heating in MRI for device implants and interventions. The localized SAR amplification at lead tips in MRI allows for the excitation of significant TAUS signals without appreciable heating. The temperature dependence of the TAUS signal in tissue makes TAUS suitable for temperature monitoring. Ultimately, TAUS acquisitions could be added to MRI sequences to provide real-time device safety information that allows more patients to have access to MRI.

ORCID

Neerav Dixit http://orcid.org/0000-0002-9437-4446

REFERENCES

1. Nitz W, Oppelt A, Renz W, Manke C, Lenhart M, Link J. On the heating of linear conductive structures as guide wires and catheters in interventional MRI. *J Magn Reson Imaging*. 2001;13:105–114.
2. Nyenhuis J, Park S, Kamondetdacha R, Amjad A, Shellock F, Rezai A. MRI and implanted medical devices: basic interactions with an emphasis on heating. *IEEE Trans Device Mater Rel*. 2005;5:467–480.
3. Shellock FG, Woods TO, Crues JV. MR labeling information for implants and devices: explanation of terminology. *Radiology*. 2009;253:26–30.
4. Nordbeck P, Weiss I, Ehses P, et al. Measuring RF-induced currents inside implants: impact of device configuration on MRI safety of cardiac pacemaker leads. *Magn Reson Med*. 2009;61:570–578.
5. Armenean C, Perrin E, Armenean M, Beuf O, Pilleul F, Hervé S. RF-induced temperature elevation along metallic wires in clinical

magnetic resonance imaging: influence of diameter and length. *Magn Reson Med*. 2004;52:1200–1206.
6. Rezai AR, Finelli D, Nyenhuis JA, et al. Neurostimulation systems for deep brain stimulation: in vitro evaluation of magnetic resonance imaging-related heating at 1.5 Tesla. *J Magn Reson Imaging*. 2002;15:241–250.
7. Baker KB, Tkach JA, Phillips MD, Rezai AR. Variability in RF-induced heating of a deep brain stimulation implant across MR systems. *J Magn Reson Imaging*. 2006;24:1236–1242.
8. Tokaya JP, Raaijmakers AJ, Luijten PR, van den Berg CA. MRI-based, wireless determination of the transfer function of a linear implant: introduction of the transfer matrix. *Magn Reson Med*. 2018;80:2771–2784.
9. Martin ET, Coman JA, Shellock FG, Pulling CC, Fair R, Jenkins K. Magnetic resonance imaging and cardiac pacemaker safety at 1.5-Tesla. *J Am Coll Cardiol*. 2004;43:1315–1324.
10. Larson P, Richardson R, Starr P, Martin A. Magnetic resonance imaging of implanted deep brain stimulators: experience in a large series. *Stereot Funct Neuros*. 2008;86:92–100.
11. Mollerus M, Albin G, Lipinski M, Lucca J. Magnetic resonance imaging of pacemakers and implantable cardioverter-defibrillators without specific absorption rate restrictions. *Europace*. 2010;12: 947–951.
12. Zrinzo L, Yoshida F, Hariz MI, et al. Clinical safety of brain magnetic resonance imaging with implanted deep brain stimulation hardware: Large case series and review of the literature. *World Neurosurgery*. 2011;76:164–172.
13. Boutet A, Rashid T, Hancu I, et al. Functional MRI safety and artifacts during deep brain stimulation: experience in 102 patients. *Radiology*. 2019;293:190546.
14. Venook RD, Overall WR, Shultz K, Conolly S, Pauly JM, Scott GC. Monitoring Induced Currents on Long Conductive Structures During MRI. In Proceedings of the 16th Annual Meeting of ISMRM, Toronto, Ontario, Canada, 2008. p. 898.
15. van den Bosch MR, Moerland MA, Lagendijk JJW, Bartels LW, van den Berg CAT. New method to monitor RF safety in MRI-guided interventions based on RF induced image artefacts. *Med Phys*. 2010;37:814–821.
16. Etezadi-Amoli M, Stang P, Kerr A, Pauly J, Scott G. Interventional device visualization with toroidal transceiver and optically coupled current sensor for radiofrequency safety monitoring. *Magn Reson Med*. 2015;73:1315–1327.
17. Griffin G, Anderson K, Celik H, Wright G. Safely assessing radiofrequency heating potential of conductive devices using image-based current measurements. *Magn Reson Med*. 2015;73:427–441.
18. Griffin GH, Ramanan V, Barry J, Wright GA. Toward in vivo quantification of induced RF currents on long thin conductors. *Magn Reson Med*. 2018;80:1922–1934.
19. Overall W, Pauly J, Stang P, Scott G. Ensuring safety of implanted devices under MRI using reversed RF polarization. *Magn Reson Med*. 2010;64:823–833.
20. Ellenor C, Stang P, Etezadi-Amoli M, Pauly J, Scott G. Offline impedance measurements for detection and mitigation of dangerous implant interactions: an RF safety prescreen. *Magn Reson Med*. 2015;73:1328–1339.
21. Rieke V, Butts Pauly K. MR thermometry. *J Magn Reson Imaging*. 2008;27:376–390.
22. Sprinkhuizen SM, Konings MK, van der Bom MJ, Viergever MA, Bakker CJ, Bartels LW. Temperature-induced tissue susceptibility changes lead to significant temperature errors in PRFS-based MR thermometry during thermal interventions. *Magn Reson Med*. 2010;64:1360–1372.
23. Gensler D, Fidler F, Ehses P, et al. MR safety: fast T_1 thermometry of the RF-induced heating of medical devices. *Magn Reson Med*. 2012;68:1593–1599.
24. Kruger RA, Liu P, Fang Y, Appledorn CR. Photoacoustic ultrasound (PAUS)-reconstruction tomography. *Med Phys*. 1995;22: 1605–1609.
25. Kruger R, Reinecke D, Kruger G. Thermoacoustic computed tomography–technical considerations. *Med Phys*. 1999;26: 1832–1837.
26. Human Röschmann P. auditory system response to pulsed radiofrequency energy in RF coils for magnetic resonance at 2.4 to 170 MHz. *Magn Reson Med*. 1991;21:197–215.
27. Dixit N, Stang PP, Pauly JM, Scott GC. Thermo-acoustic ultrasound for detection of RF-induced device lead heating in MRI. *IEEE Trans Med Imaging*. 2018;37:536–546.
28. Fan Y, Mandelis A, Spirou G, Alex Vitkin I. Development of a laser photothermoacoustic frequency-swept system for subsurface imaging: theory and experiment. *J Acoustical Soc Am*. 2004;116:3523–3533.
29. Shah J, Park S, Aglyamov SR, et al. Photoacoustic imaging and temperature measurement for photothermal cancer therapy. *J Biomed Opt*. 2008;13:034024.
30. Pramanik M, Wang LV. Thermoacoustic and photoacoustic sensing of temperature. *J Biomed Opt*. 2009;14:054024.
31. Lou C, Xing D. Temperature monitoring utilising thermoacoustic signals during pulsed microwave thermotherapy: a feasibility study. *Int J Hyperthermia*. 2010;26:338–346.
32. Ke H, Erpelding TN, Jankovic L, Wang LV. Temperature mapping using photoacoustic and thermoacoustic tomography. In Proceedings SPIE 8223, Photons Plus Ultrasound: Imaging and Sensing 2012, San Francisco, California, USA, 2012. p. 82330.
33. Xu F, Ji Z, Chen Q, Yang S, Xing D. Nonlinear thermoacoustic imaging based on temperature-dependent thermoelastic response. *IEEE Trans Med Imaging*. 2019;38:205–212.
34. Zanchi M, Venook R, Pauly J, Scott G. An optically coupled system for quantitative monitoring of MRI-induced RF currents into long conductors. *IEEE Trans Med Imaging*. 2010;29:169–178.
35. Stollberger R, Wach P. Imaging of the active B_1 field in vivo. *Magn Reson Med*. 1996;35:246–251.
36. Preiswerk F, Toews M, Cheng CC, et al. Hybrid MRI-Ultrasound acquisitions, and scannerless real-time imaging. *Magn Reson Med*. 2017;78:897–908.
37. Ghanouni P, Pauly KB, Elias WJ, et al. Transcranial MRI-guided focused ultrasound: a review of the technologic and neurologic applications. *Am J Roentgenol*. 2015;205:150–159.
38. Almquist S, Parker DL, Christensen DA. Rapid full-wave phase aberration correction method for transcranial high-intensity focused ultrasound therapies. *J Therapeutic Ultrasound*. 2016; 4:30.
39. Huang L, Li T, Jiang H. Thermoacoustic imaging of hemorrhagic stroke: a feasibility study with a human skull. *Med Phys*. 2017;44:1494–1499.
40. Yan A, Lin L, Liu C, Shi J, Na S, Wang LV. Microwave-induced thermoacoustic tomography through an adult human skull. *Med Phys*. 2019;46:1793–1797.
41. Pennes HH. Analysis of tissue and arterial blood temperatures in the resting human forearm. *J Appl Physiol*. 1948;1:93–122.

How to cite this article: Dixit N, Pauly JM, Scott GC, et al. Thermo-acoustic ultrasound for noninvasive temperature monitoring at lead tips during MRI. *Magn Reson Med*. 2019;00:1–13. https://doi.org/10.1002/mrm.28102

APPENDIX A

For the scenario described in Section 2.2 and Figure 3 in which current is driven into a spherical electrode immersed in homogeneous tissue, the worst-case (no perfusion and no heat flow from the tissue into the electrode) steady-state temperature rise ΔT caused by a constant current level can be analytically derived by considering Pennes' bioheat transfer equation[41]

$$\rho C_p \frac{\partial(\Delta T)}{\partial t} = \nabla \cdot k \nabla(\Delta T) + \rho \mathrm{SAR} - W_{bl} C_{bl} \left(T - T_{bl}\right) + q_m. \quad \text{(A1)}$$

Here, ρ, C_p, and k, respectively, describe the density, the specific heat, and the thermal conductivity of the tissue. SAR is the power absorption density resulting from the current, W_{bl} is the tissue-blood perfusion rate, C_{bl} is the specific heat of the blood, T_{bl} is the blood temperature, and q_m describes metabolic heat generation.

Ignoring perfusion, assuming metabolic heating effects are negligible relative to the effects from the current, and setting the temporal derivative to zero to obtain a steady-state solution allows the equation to be simplified to

$$-k\nabla^2(\Delta T) = \rho \mathrm{SAR}. \quad \text{(A2)}$$

Substituting in the SAR from Equation 3 and noting the radial symmetry in this scenario when evaluating $\nabla^2 T$ gives

$$-k\frac{1}{r^2}\frac{\partial}{\partial r}\left(r^2\frac{\partial \Delta T}{\partial r}\right) = \frac{I_{\mathrm{rms}}^2}{16\pi^2\sigma r^4}. \quad \text{(A3)}$$

Multiplying both sides of this equation by r^2 and integrating results in

$$kr^2\frac{\partial \Delta T}{\partial r} = \frac{I_{\mathrm{rms}}^2}{16\pi^2\sigma r} + C_0, \quad \text{(A4)}$$

where C_0 is an integration constant. Dividing both sides of this equation by kr^2 and integrating again gives

$$\Delta T = -\frac{1}{2}\frac{I_{\mathrm{rms}}^2}{16\pi^2 k\sigma r^2} - \frac{C_0}{kr} + C_1, \quad \text{(A5)}$$

where C_1 is another integration constant. Since ΔT approaches zero as r approaches infinity, $C_1 = 0$. By assuming that no heat flow occurs between the tissue and the electrode ($\partial \Delta T/\partial r = 0$ at $r = R_0$), the integration constant C_0 can be solved in Equation A4, yielding Equation 4.